Aalborg Universitet

Diagnosis of Lithium-Ion Batteries State-of-Health based on Electrochemical Impedance Spectroscopy Technique

Stroe, Daniel Ioan; Swierczynski, Maciej Jozef; Stan, Ana-Irina; Knap, Vaclav; Teodorescu, Remus; Andreasen, Søren Juhl

Diagnosis of Lithium-Ion Batteries State-of-Health based on Electrochemical Impedance Spectroscopy Technique

Daniel I. Stroe, Maciej Swierczynski, Ana I. Stan, Vaclav Knap, R. Teodorescu, Søren J. Andreasen

Department of Energy Technology, Aalborg University
Aalborg, Denmark
dis@et.aau.dk

Abstract—**Lithium-ion batteries have developed into a popular energy storage choice for a wide range of applications because of their superior characteristics in comparison to other energy storage technologies. Besides modelling the performance behavior of Lithium-ion batteries, it has become of huge interest to accurately diagnose their state-of-health (SOH). At present, Lithium-ion batteries are diagnosed by performing capacity or resistance (current pulse) measurements; however, in the majority of the cases, these measurements are time consuming and result in changing the state of the battery as well. This paper investigates the use of the electrochemical impedance spectroscopy (EIS) technique for SOH diagnosis of Lithium-ion battery cells, instead of using the aforementioned techniques, since this new method allows for online and direct measurement of the battery cell response in any working point. For the investigation, a 2.5 Ah Lithium-ion battery cell based on lithium iron phosphate and graphite (LiFePO$_4$/C), as active material, was used. The obtained results at different battery SOH levels have been analyzed in detail and are suggesting that the EIS technique represents a promising tool for diagnosis the lithium-ion battery cells' SOH; meaningful results regarding the pulse power capability decrease of the tested Li-ion battery cells were obtained by applying the EIS technique.**

I. INTRODUCTION

Lithium-ion (Li-ion) batteries had continuously improved their performances in the last decade; present Li-ion batteries are characterized by high power capability, long calendar and cycle lifetime, high efficiency and intrinsic safety [1]. Thus, the Li-ion battery technology is considered a suitable alternative to other energy storage technologies (e.g. lead acid batteries, supercapacitors etc.) for a wide range of applications such as renewables' grid integration, grid services, automotive industry and UPS systems [2] – [5].

Once with the use of Li-ion batteries at a large scale, a lot of research interest is focusing on their performance and degradation monitoring and estimation [6] – [8]. However, these tasks are not straightforward, mainly because the degradation mechanisms of Li-ion batteries are complex and not completely understood yet [9]. Li-ion batteries are characterized by a high non-linear behaviour since their performance parameters (i.e. voltage, capacity, internal resistance, and power capability) are dependent on the operating conditions (i.e. temperature, state-of-charge, and load current) [10], [11]; moreover, the performances of the Li-ion batteries are changing with their state-of-health (SOH) [12].

In real applications, accurate estimation and fast and reliable SOH diagnosis of the Li-ion batteries could reduce or even avoid downtime periods of the battery systems, which are necessary for maintenance and/or replace operations. Depending on the targeted information, the measurement techniques that are commonly used to diagnose the SOH of Li-ion batteries are capacity measurements, efficiency measurements, and internal resistance (current pulse) measurements.

The focus of this paper is to investigate if the electrochemical impedance spectroscopy (EIS) represents a suitable technique for diagnosis of Li-ion batteries SOH. For this investigation, 2.5 Ah Li-ion batteries (with lithium iron phosphate and graphite as active materials) were used.

II. ELECTROCHEMICAL IMPEDANCE SPECTROSCOPY

EIS technique represents a non-destructive and reliable method that can be applied for characterizing and modelling the dynamic behavior of Li-ion batteries [13]. This measurement technique allows developing dynamic battery cell models whose elements can be often correlated to the physic-chemical processes that occur inside the battery cell (e.g. charge transfer, diffusion etc.) [13], [14].

The measurement approach consists in applying to the battery a sinusoidal current or voltage of a certain amplitude and frequency and measuring the phase shift and amplitude of the output voltage (galvanostaic mode) or current (potentiostatic mode), respectively [13], [15]. This procedure is usually repeated for a number of frequencies and thus the impedance spectrum of the investigated battery is derived.

Most frequently, the results of the EIS measurement are presented in the Nyquist plane, where the inverse of the imaginary part of the impedance is plotted against its real part. The general shape of Li-ion batteries' Nyquist diagram (also referred in literature as impedance characteristic or impedance spectra) is presented in Fig. 1.

The impedance spectra presented in Fig. 1 is composed of five distinct sections which in literature are related to different processes: at very high frequencies, the impedance spectra shows an inductive behavior (inductance L_s); the value of the ohmic resistance R_s of the battery is found at the intersection of the impedance spectra with the real axis ($Im(Z) = 0$); the third section is represented by a small semi-circle which is related with the presence of the solid electrolyte interface (SEI) layer; the larger semi-circle (fourth section) is associated with the charge transfer process and the double layer capacitance; the fifth section, located at small frequencies, corresponds to the diffusion process.

Usually, the measured Nyquist diagrams are fitted using a complex non-linear least square (CNLS) algorithm and considering an equivalent electrical circuit (EEC), similar to the circuit presented in Fig. 2, in order to build accurate impedance-based performance models. However, this is out of the scope of this paper whose aim is to investigate to what extent the EIS technique (and subsequently the parameters of the EEC) could be used to diagnose the degradation (SOH) of Li-ion battery cells.
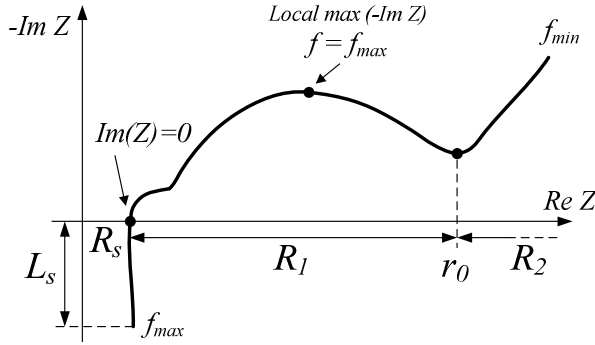

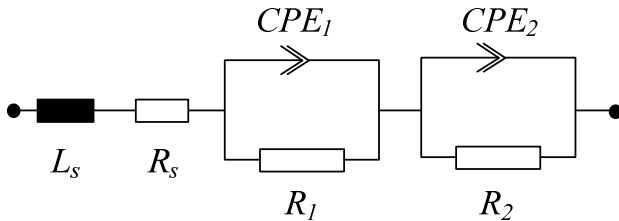Figure 1.   Typical Nyquist diagram of Li-ion batteries.

Figure 2.   Typical equivalent electrical circuit used for curve fitting the Nyquist diagram of Li-ion batteries.

III.   EXPERIMENT DESCRIPTION

A. Accelerated Ageing Tests

Ageing of the considered Li-ion battery cells at normal operating conditions is a time and resource consuming process. Thus, in order to obtain a relative fast degradation of the Li-ion battery cells, accelerated cycling ageing tests were performed in laboratory conditions. The accelerated cycling ageing was obtained by considering a high cycling temperature (50 °C) and high cycling current rate (4C-rate). Moreover, in order to obtain more meaningful data, the battery cells were cycled considering three different cycle depths. Table I summarizes the tests conditions for the three considered cases.

TABLE I.   ACCELERATED CYCLING AGEING CONDITIONS

Test case name	Cycle depth	SOC interval	Temperature	C-rate/ Current
TC 1	10 %	45% - 55%		
TC 2	35 %	32.5% - 67.5%	50 °C	4 C-rate (10A)
TC 3	60 %	20 % - 80%		

EIS measurements were performed before starting the accelerated ageing procedure and periodically thereafter at certain time intervals (after each 3250, 950, and 550 cycles for TC1, TC2, and TC3, respectively) until the battery cells reached their end-of-life (EOL). The accelerated ageing tests were stopped when the tested Li-ion battery cells had achieved their EOL, which was predefined at 20% capacity fade.

B. Impedance characteristic of the tested Li-ion battery cell

All the EIS measurements were performed in galvanostatic mode, for the frequency range 10 kHz – 10 mHz, at 25°C, and at three different SOC levels, 20%, 50%, and 80%, without superimposed DC current. Moreover, all the EIS measurements were performed considering two measurement periods for each frequency and four seconds measuring time. The measuring time is an extremely important parameter since is directly related to the noise rejection during the measurement (e.g., a 4 times longer measuring time will reduce the noise with a factor of 2).

The impedance spectrum of the tested battery cell, which was measured at the beginning-of-life (BOL) is presented in Fig. 3. Its shape differs from the shape present in Fig 1, since the shape of the impedance spectra varies depending on the chemistry of the Li-ion battery cell.

In order to eliminate possible outliers and to avoid sudden-death of the battery cells, three cells were tested for each of the three considered accelerated cycling ageing conditions that are presented in Table I. Fig. 4 presents the impedance spectra measured, at the BOL and EOL, on the three cells tested under TC3 conditions. As it can be observed, extremely similar Nyquist diagrams were measured at both BOL and EOL for the three cells; therefore, the average of the curves was obtained and used in the further analysis of the ageing results.
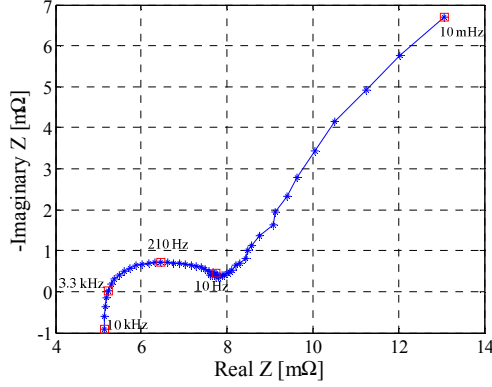
Figure 3. Measured impedance spectra of the tested Li-ion battery cell; measurement performed at BOL, 25 °C, 50% SOC.
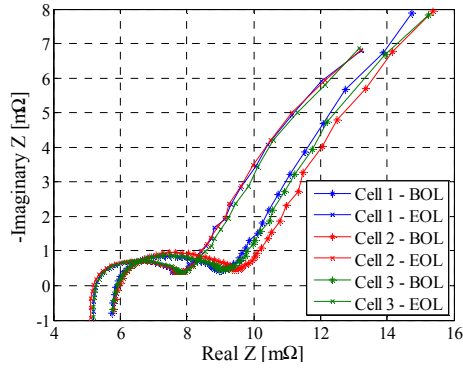
Figure 4. Measured impedance spectra at BOL and EOL (25 °C, 50% SOC) for battery cells aged under TC3 conditions.

IV. RESULTS

A. Dependence of the battery impedance characteristic on the SOC at various SOH levels

In this subsection, the dependence of the battery impedance spectra on the SOC and its variation with SOH is discussed.

In Fig. 5, the measured impedance spectra of cells tested under TC1, TC2, and TC3 conditions are shown for three different SOC levels (i.e. 20%, 50% and 80%) at BOL and EOL. The shape of the measured impedance spectra of the tested Li-ion battery cells has remained basically unchanged for fresh (BOL) and aged (EOL) cells independent on the ageing conditions which were applied to the batteries. Moreover, for all the fresh cells, a decrease of the first semi-circle can be observed (especially on the zoom view of the plots from Fig. 5) with the increase of the SOC level, which corresponds to a decrease of the value of resistance R_1; the same trend has been observed for aged cells, independent on the applied accelerated ageing test.

These results and dependences are mostly valid for the tested Li-ion battery chemistry (e.g. LiFePO$_4$/C) and could change depending on the chemistry of the tested Li-ion battery. For example, Eddahech et al. present in [16] results from EIS measurements on a fresh Li-ion battery cell, based on the NMC chemistry; for this particular cell, both the intersection point of the impedance spectra with the X-axis (R_s) and the size of the first semi-circle (R_1) are changing with SOC.

Figure 5. Measured impedance characteristic at BOL (top) and EOL (bottom) for battery cells tested under TC1 (left), TC2 (centre), and TC3 (right) conditions.

B. Dependence of the battery impedance on the SOH
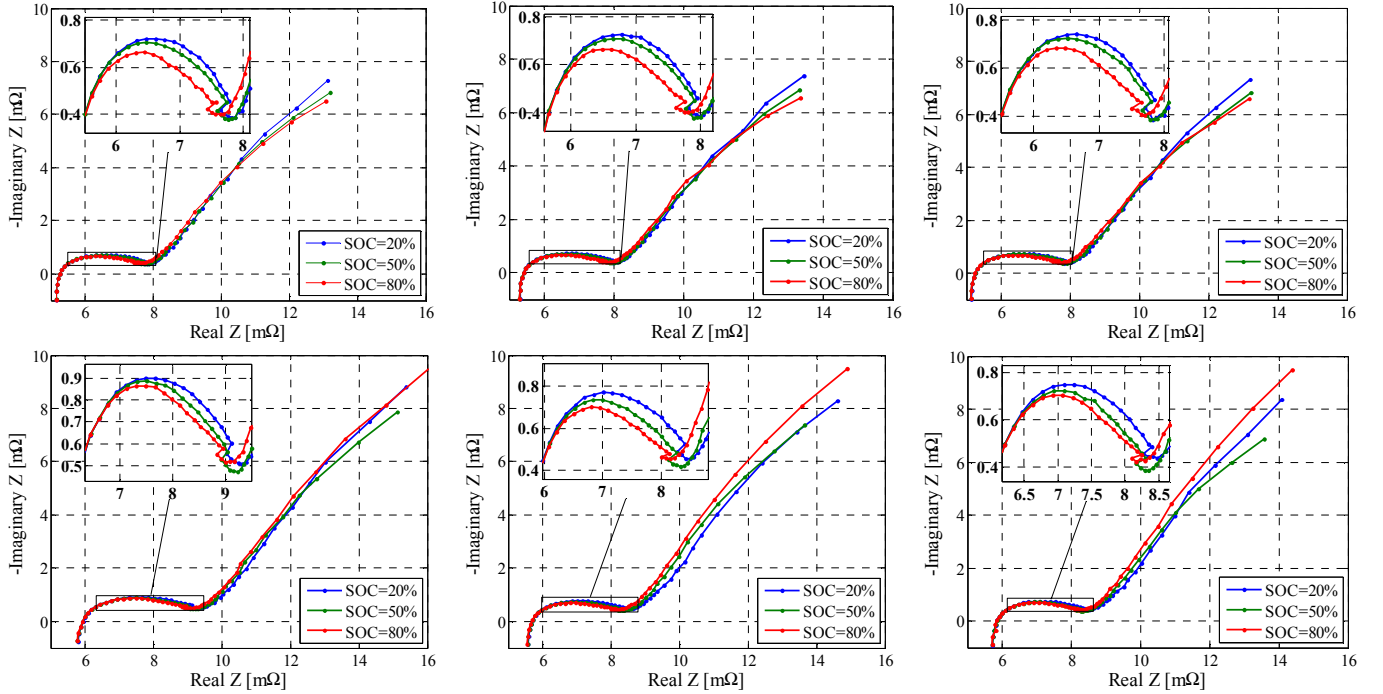
In this subsection, the dependence of the tested Li-ion battery impedance spectra on the SOH is analyzed. In Fig. 6, the evolution of the impedance spectra during the ageing process is presented for the three considered ageing TCs. Generally, the measured impedance spectra of the tested Li-ion batteries were shifted to the right side of the Nyquist plane, while the ageing process has evolved. This shift corresponds mainly to the increase of the ohmic resistance R_s while the Li-ion battery cell is ageing. No other changes/trends were observed at the visual inspection of the measured impedance spectra. These results are in good agreement with the results obtained from accelerated calendar ageing tests, which are presented in [17] for the same Li-ion battery chemistry.

The Nyquist diagrams presented in Fig. 5 were measured at 50% SOC; however, similar ageing trends were obtained for the Nyquist diagrams measured at 20% SOC and 80% SOC.
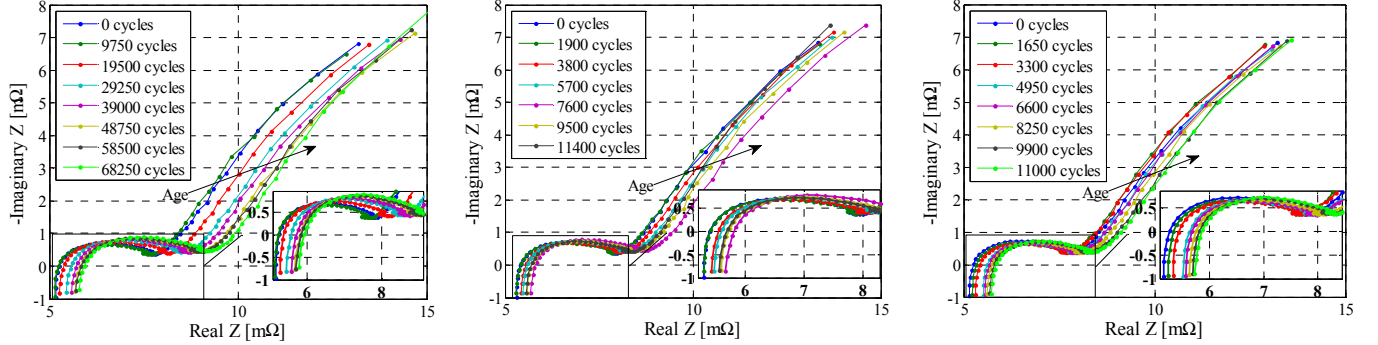

Figure 6. Change of the impedance characteristic during battery cells' life-span for different ageing conditions:TC1 (left), TC2 (centre), and TC3 (right) – (measurements performed at T=25°C and SOC=50%).

C. Variation of the equivalent electrical circuit parameters with the SOH

This subsection provides a detailed analysis of how the parameters of the EEC, which was used for curve fitting the measured impedance spectra, have been influenced by the ageing process.

By applying a CNLS algorithm, the Nyquist diagrams measured throughout the accelerated ageing TCs were fitted using the EEC shown in Fig. 2. The circuit is composed of a series inductance L_s, a series resistance R_s, and two ZARC elements; ZARC elements are a parallel connection of a resistor and a constant phase element (CPE) [6]. CPEs are characterized by a generalized capacitance Q and a depression factor n and are defined as:

$$Z_{CPE} = \frac{1}{j\omega^n Q} \qquad (1)$$

For a depression factor equal to 1, the CPE will behave similar to a capacitor.

During the fitting process, the values of the parameters L_s, N_1 and N_2 were kept fixed at $1.884 \cdot 10^{-8}$ H, 0.65, and 0.67, respectively, while the parameters R_s, R_1, R_2, Q_1, and Q_2 were considered variable. After an initial evaluation of the values obtained for the parameters which were considered variable, it was observed that the values of the parameters R_s, R_1, R_2, and Q_2 are following certain trends and are meaningful to be further analyzed. For the values of the generalized capacitance Q_1, which had been obtained from the fitting processes, no obvious dependence were found neither on SOC nor on SOH, independent on the considered TC.

The increase of the ohmic resistance R_s due to ageing is illustrated in Fig. 7. As it may be observed, the values of the ohmic resistance are not changing with the SOC value which is in good agreement with the results presented in Fig. 4. Moreover, this dependency of R_s on SOC remains unchanged throughout the entire ageing process and is not dependent on the ageing conditions. The increase of the R_s during the ageing tests is rather reduced and varies between 8% and 14%, depending on the considered TC.

The increase of the resistance R_1, and subsequently of the SEI layer, during the performed accelerated ageing TCs is presented in Fig. 8. As already mentioned, the measured values of resistance R_1 are increasing linearly with decreasing of the SOC in the interval 20%-80%. Furthermore, similar to the case of the ohmic resistance, this dependence of R_1 on SOC remains unchanged during the Li-ion battery cells' ageing, independent on the applied accelerated ageing conditions (see also Fig. 5).

Fig 9 presents the increase of the measured charge transfer resistance R_2, at various SOH levels, during the battery cells' ageing process. At the BOL, a linear dependence between resistance R_2 and SOC (for the interval 20%-80%) was observed; however, once the ageing process was advancing, this dependence had become parabolic and more pronounced for SOH levels close to battery cells' EOL. As shown in Fig. 9, the same ageing behavior of the resistance R_2 was found independent on the considered

ageing conditions. Moreover, the increase of the R_2 parameter, caused by the cycling ageing, is the most pronounced (i.e. 25% – 90%) among the increasing levels of the resistances of the EEC.

The decrease of the generalized capacitance Q_2 obtained during the three accelerated cycling ageing tests is presented in Fig. 10. A slight parabolic dependence of the Q_2 parameter on the SOC was measured at the cells' BOL; afterwards, this parabolic dependence has become more pronounced, especially for high SOC levels (i.e. 80%), while the ageing process had evolved.
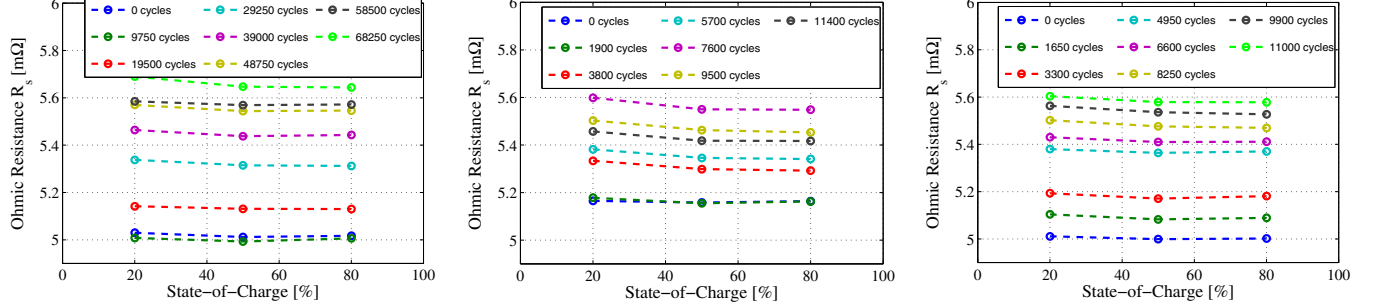

Figure 7. Dependence of the ohmic resistance R0 on the SOC at different ageing periods, measured during battery cells ageing under TC1 (left), TC2 (middle), and TC3 (right) conditions.
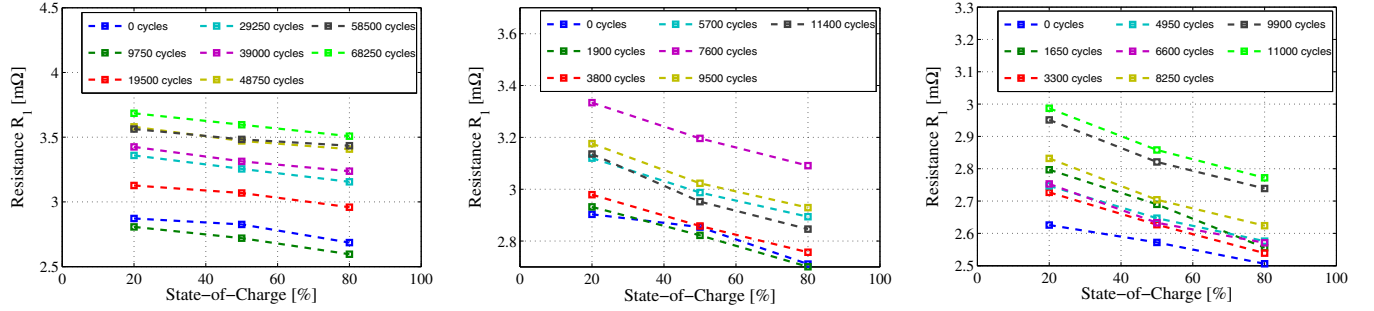

Figure 8. Dependence of resistance R1 on the SOC at different ageing periods, measured during battery cells ageing under TC1 (left), TC2 (middle), and TC3 (right) conditions.
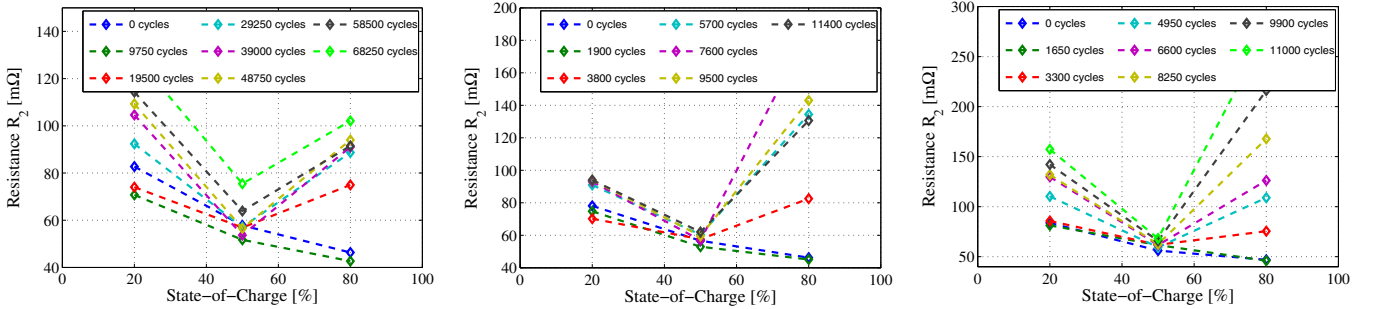

Figure 9. Dependence of charge transfer resistance R2 on the SOC at different ageing periods, measured during battery cells ageing under TC1 (left), TC2 (middle), and TC3 (right) conditions.
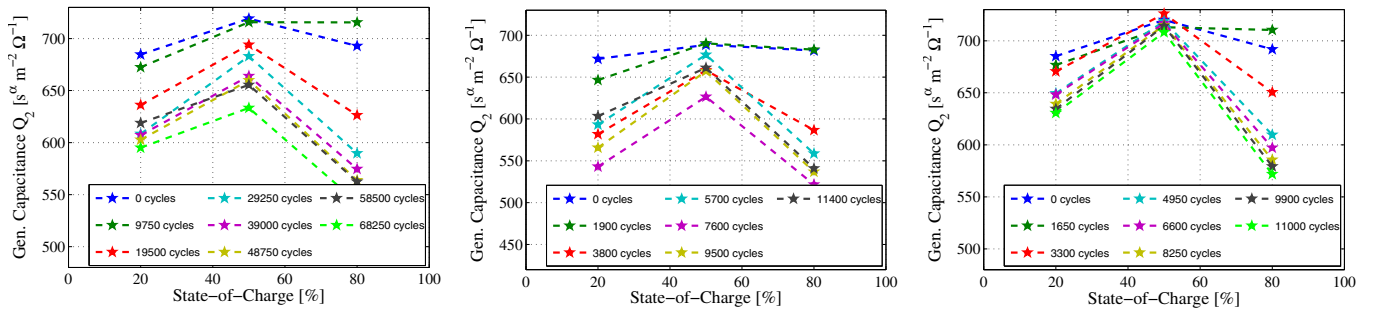

Figure 10. Dependence of generalized capacitance Q_2 on the SOC at different ageing periods, measured during battery cells ageing under TC1 (left), TC2 (middle), and TC3 (right) conditions.

D. Diagnosis of Li-ion battery SOH based on EIS technique

Furthermore, it has been found out that the increase of the ohmic resistance R_s and of the charge transfer resistance R_2 obtained at various SOH levels of the battery, during the considered degradation processes could be modelled as function of number of cycles and their corresponding cycle depths.

The increase of R_s, as function of number of cycles, was fitted separately for the three considered ageing conditions using a power function (2), as presented in Fig. 11; among different explored fitting functions, the power function has returned the best fitting accuracy.

$$R_{s,inc}\,[\%] = a_1 \cdot nc^{a_2} \qquad (2)$$

where a_1 represents the coefficient of the power function, a_2 represents the exponent of the power function and nc represents the number of cycles.

The fitting results of the R_s increase as function of number of cycles for the three TCs as well as the fitting accuracy (given by the coefficient of determination R^2) are summarized in Table II.

TABLE II. DEPENDENCE OF RS INCREASE ON THE CYCLING CONDITIONS

Test Case	Fitting Results		
	a_1	a_2	R^2
TC1	$2.632 \cdot 10^{-5}$	1.188	0.918
TC2	0.001733	0.906	0.804
TC3	0.00678	0.851	0.976

Moreover, it was found out that there is a second power dependence between the parameters a_1 and a_2 and the cycle depths at which the cycle ageing was performed. The final ageing model obtained for the ohmic resistance is given in (3). Following the same approach, the ageing model for the charge transfer resistance increase (see Fig. 12) was also derived and is given in (4).

$$R_{s,inc}[\%] = 3.766 \cdot 10^{-8} \cdot cd^{2.958} \cdot nc^{1.852 \cdot cd^{-0.1947}} \qquad (3)$$

$$R_{2,inc}[\%] = 1.459 \cdot 10^{-14} \cdot cd^{5.138} \cdot nc^{3.14 \cdot cd^{-0.1559}} \qquad (4)$$

where, $R_{2,inc}$ represents the increase of resistance R_2, and cd represents the cycle depth.

Based on the ageing models (3) and (4), the increase of the resistances R_s and R_2 can be estimated for cycling the considered Li-ion batteries at high temperature (50°C) with different load profiles.

Fig. 13 presents the relationships between the increase of the ohmic resistance (values obtained from EIS measurements) and the decrease of the discharge pulse power capability (values obtained from HPPC

measurements) throughout the degradation process of the Li-ion battery cells, for the three TCs, respectively. These relationships obtained for the performed TCs (given by (5) – (7)) are showing a linear dependence between the two parameters. Therefore, it can be concluded that the ageing mechanisms responsible for the ohmic resistance increase is responsible for the power capability decrease as well. Furthermore, it can be concluded that the EIS technique can be used for SOH diagnosis of the tested battery cells since it can give reliable information about Li-ion cells' pulse power capability decrease.

$$DPPC_{TC1} = 0.074 \cdot R_{s,TC1} + 0.075 \qquad (5)$$

$$DPPC_{TC2} = 0.105 \cdot R_{s,TC2} + 0.118 \qquad (6)$$

$$DPPC_{TC3} = 0.871 \cdot R_{s,TC3} - 0.075 \qquad (7)$$

where, $DPPC_{TC1}$, $DPPC_{TC2}$, $DPPC_{TC3}$ represent the discharge pulse power capabilities measured using the HPPC technique for the cells aged under TC1, TC2, and TC3 conditions respectively; $R_{s,TC1}$, $R_{s,TC2}$ and, $R_{s,TC3}$ represent the ohmic resistances obtained by curve fitting the Nyquist diagrams measured on the cells aged under TC1, TC2, and TC3 conditions.
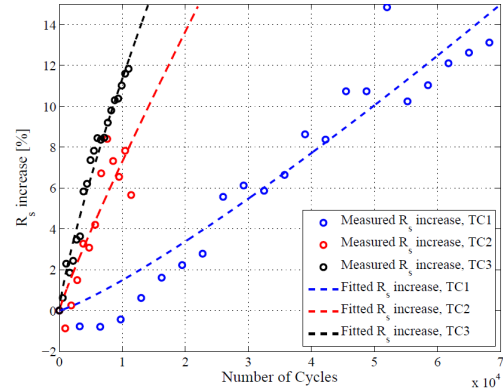

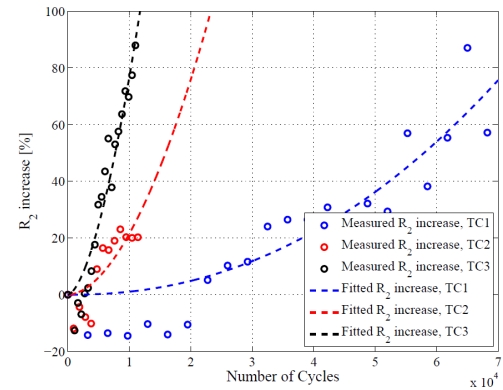Figure 11. Measured and fitted R_s increase obtained for different accelerated ageing conditions.

Figure 12. Measured and fitted R_2 increase obtained for different accelerated ageing conditions.
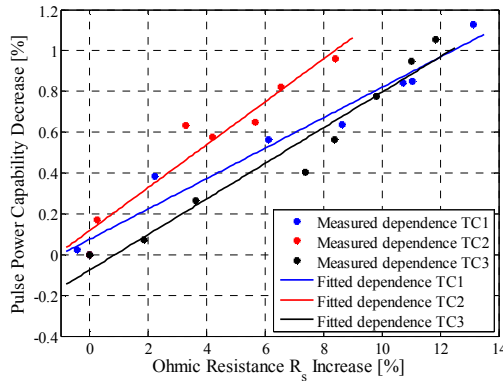
Figure 13. Relation between R_s increase and the discharge pulse power capability decrease (SOC=20%).

V. CONCLUSIONS

This paper has investigated the suitability of using the EIS technique to diagnose the degradation of Li-ion battery cells; for this investigation 2.5 Ah lithium iron phosphate/graphite battery cells were used.

In order to perform this investigation, accelerated ageing tests were performed in laboratory until the cells had achieved their EOL (20% capacity fade); periodically, during the accelerated ageing TCs, EIS measurements were performed. The influence of ageing on the parameters of the EEC, which has been used to fit the Nyquist diagrams, was analysed; the parameters R_s, R_1, R_2, Q_1, and Q_2 have been found to vary with the ageing, but only the resistances and the generalized capacitance Q_2 have shown a relevant ageing trend. Even though the values of R_s, R_1, and, R_2 have increased during the ageing process, the most obvious increase (between 25% and 90%, depending on the TC) was observed for R_2. The linear dependence on SOC (for the SOC interval 20%-80%) of R_s and R_1 was not changing with the battery cells' SOH while the dependence of R_2 on SOC evolves from linear (at BOL) to parabolic (at EOL). Finally, it was determined that the increase of the ohmic resistance during ageing can be correlated with the decrease of the Li-ion battery cells' pulse power capability. Thus, the EIS technique can be used to diagnose the SOH, in terms of power capability decrease, of the tested Li-ion batteries.

Nevertheless, the reader should remember that the presented results were obtained for LiFePO$_4$-based battery cells and the derived dependences and trends could differ significantly for Li-ion battery cells based on other chemistries.

REFERENCES

[1] B. Scrosati, J. Garche, "Lithium batteries: Status, prospects and future," Journal of Power Sources, 195 (2010) 2419-2430.

[2] T. Ackermann, "Wind Power in Power Systems", 2nd edition, Wiley, 2012.

[3] S. Vazquez, S. Lukic, E. Galvan, L.G. Franquelo, J.M. Carrasco, "Energy Storage Systems for Transport and Grid Applications," *IEEE Transactions on Industrial Electronics*, vol. 57, no. 12, Dec. 2010, p. 3881-3895.

[4] S. Lansburg, C. Jehoulet, "Innovative modular Li-ion battery system delivers high power support for data centre UPS installations", IEEE Telecommunications Energy Conference 'Smart Power and Efficiency' (INTELEC), Proceedings of 2013 35th International, pp.1-6, 13-17 Oct. 2013, Hamburg, Germany;

[5] M. Swierczynski et al. "Field tests experience from 1.6MW/400kWh Li-ion battery energy storage system providing primary frequency regulation service," IEEE 2013 ISGT-Europe, pp. 1-5, 7-9 Oct. 2013, Copenhagen, Denmark.

[6] M. Swierczynski, D.I. Stroe, A.I. Stan, R. Teodorescu, D.U. Sauer, "Selection and Performance-Degradation Modeling of LiMO$_2$/Li$_4$Ti$_5$O$_{12}$ and LiFePO$_4$/C Battery Cells as Suitable Energy Storage Systems for Grid Integration With Wind Power Plants: An Example for the Primary Frequency Regulation Service, " IEEE transactions on Sustianable Energy, vol. 5, no. 1, Jan. 2014, pp. 90-101.

[7] D.I. Stroe, M. Swierczynski, A.I. Stan, R. Teodorescu, S.J. Andreasen, "Accelerated lifetime testing methodlgy for lifetime estimation of lithium-ion batteries used in augmented wind power plants," IEEE Transactions on Industry Applications, 2014.

[8] J. Groot, "State-of-health estimation of Li-ion batteries: cycle life test methods," Licentiate Thesis, Chalmers University of Technology, 2012.

[9] J. Vetter et al., "Ageing mechanisms in lithium-ion batteries," Journal of Power Sources, 147 (2005) 269-281.

[10] M. Chen, A. Rincon-Mora, "Accurate electrical battery model capabale of predicting runtime and I-V performance," IEEE Transactions on Energy Conversion, vol. 21, no. 2, pp. 504-511, June 2006.

[11] L. Gao, S. Liu, R. A. Dougal, "Dynamic lithium-ion battery model for system simulation," IEEE transactions on Components and Packaging Technologies, vol. 25, no. 3, pp. 495-505, Sept 2002.

[12] D.I. Stroe, D.I. Stroe, M. Swierczynski, A.I. Stan, R. Teodorescu, "Accelerated lifetime testing methodlgy for lifetime estimation of lithium-ion batteries used in augmented wind power plants," Energy Conversion Congress and Exposition (ECCE), 2013 IEEE, pp. 690-698, 15-19 Oct 2013, Denver, U.S.

[13] E. Barsoukov and J.R. Macdonald, "Impedance Spectroscopy. Theory, Experiment and Applications," Wiley 2005.

[14] E. Karden, S. Buller, R.W. De Doncker, "A frequency-domain approach to dynamical modeling of electrochemical power sources," Electrochemical Acta 47 (2002) 2347-2356.

[15] S. Buller, M. Thele, R.W. De Doncker, E. Kardem, "Impedance-Based Simulation Models of Supercapacitors and Li-Ion Batteries for Power Electronic Applications," IEEE Transactions on Industry Applications, vol. 41, no. 3, May 2005.

[16] A. Eddahech et al., "Lithium-ion cell modelling from impedance spectroscopy for EV applications," Energy Conversion Congress and Exposition (ECCE), 2011 IEEE, 17-22 Sept 2013, Phoenix, U.S.

[17] M. Kassem et al., "Calendar ageing of a graphite/LiFePO$_4$ cell," Journal of Power Sources 208 (2012) 296-305.